Cysteine Mutagenesis Reveals Novel Structure–Function Features within the Predicted Third Extracellular Loop of the Type IIa Na^+/P_i Cotransporter

Georg Lambert, Ian C. Forster, Gerti Stange, Katja Köhler, Jürg Biber, and Heini Murer

From the the Institute for Physiology, University of Zürich, CH-8057, Zürich, Switzerland

ABSTRACT The transport function of the rat type IIa Na^+/P_i cotransporter is inhibited after binding the cysteine modifying reagent 2-aminoethyl methanethiosulfonate hydrobromide (MTSEA) to a cysteine residue substituted for a serine at position 460 (S460C) in the predicted third extracellular loop. This suggests that Ser-460 lies in a functionally important region of the protein. To establish a "structure–function" profile for the regions that flank Ser-460, the substituted cysteine accessibility method was employed. 18 mutants were constructed in which selected amino acids from Arg-437 through Leu-465 were substituted one by one for a cysteine. Mutants were expressed in *Xenopus* oocytes and transport function (cotransport and slippage) and kinetics were assayed by electrophysiology with or without prior treatment with cysteine modifying (methanethiosulfonate, MTS) reagents. Except for mutant I447C, mutants with cysteines at sites from Arg-437 through Thr-449, as well as Pro-461, were inactive. Cotransport function of mutants with Cys substitutions at sites Arg-462 through Leu-465 showed low sensitivity to MTS reagents. The preceding mutants (Cys substitution at Thr-451 to Ser-460) showed a periodic accessibility pattern that would be expected for an α-helix motif. Apart from loss of transport function, exposure of mutants A453C and A455C to MTSEA or 2-(triethylammonium)ethyl MTS bromide (MTSET) increased the uncoupled slippage current, which implicated the mutated sites in the leak pathway. Mutants from Ala-453 through Ala-459 showed less pH dependency, but generally stronger voltage dependency compared with the wild type, whereas those flanking this group were more sensitive to pH and showed weaker voltage dependence of cotransport mode kinetics. Our data indicate that parts of the third extracellular loop are involved in the translocation of the fully loaded carrier and show a membrane-associated α-helical structure.

KEY WORDS: cysteine scanning • electrophysiology • mutagenesis • phosphate transport • secondary structure

INTRODUCTION

The proteins responsible for transport of inorganic phosphate (P_i)[1] in mammals have been classified into three types (I, II, and III). They differ in primary structure, tissue localization, and functional properties (for review, see Murer et al., 2000). The type IIa Na^+/P_i cotransporter (NaPi-IIa) is primarily responsible for P_i reabsorption at the brush border membrane of the renal proximal tubule, and it therefore plays an important role for the maintenance of mammalian P_i homeostasis. NaPi-IIa isoforms from several species have been cloned and expressed in *Xenopus laevis* oocytes, and their transport kinetics have been characterized in detail (Busch et al., 1994, 1995; Hartmann et al., 1995; Forster et al., 1998, 2000). The key functional features are: Na^+-dependent P_i cotransport (3:1 Na^+/P_i stoichiometry, Forster et al., 1999a), ordered substrate binding (Na^+ - $P_I{}^{2-}$ - $2Na^+$, Forster et al., 1998), substrate specificity (divalent P_i is the preferred species, Forster et al., 1999a), voltage-dependent transport (one net charge transfer per transport cycle, Busch et al., 1994; Forster et al., 1998), P_i-independent Na^+ slippage (Forster et al., 1998), and intrinsic pH sensitivity independent of P_i species (suppressed P_i transport with acidification, Busch et al., 1994, 1995; Forster et al., 1999a, 2000). The multiplicity of these kinetic features suggests that they are conferred by specific, unique structural elements and/or motifs, the identification of which is the current challenge in structure–function studies on the NaPi-IIa protein.

The rat NaPi-IIa isoform is a 637 amino acid protein. The original hydrophobicity analysis (Magagnin et al., 1993; see also Murer et al., 2000), together with recent antibody accessibility studies (Lambert et al., 1999b) and cysteine scanning approaches (Lambert et al., 2000a,b), support a secondary structure topology that comprises eight transmembrane domains, a large extra-

Drs. Lambert and Forster contributed equally to this work and should be considered co-first authors.

Address correspondence to Ian C. Forster, Ph.D., Physiologisches Institut, Universität Zürich-Irchel Winterthurerstr. 190, CH-8057 Zürich, Switzerland. Fax: 41-1-635 5715; E-mail: iforster@access.unizh.ch

[1]*Abbreviations used in this paper:* ECL-3: third extracellular loop; MTS, methanethiosulfonate; MTSEA, 2-aminoethyl MTS hydrobromide; MTSET, 2-(triethylammonium)ethyl MTS bromide; NaPi-IIa, type IIa sodium phosphate cotransporter; PFA phosphonoformic acid; P_i, inorganic phosphate; SCAM, substituted cysteine accessibility method; TMD, transmembrane domain; WT, wild type.

cellular loop with two glycosylation sites (Hayes et al., 1994), and intracellular NH_2 and COOH termini (Lambert et al., 1999b). Until recently, nothing had been established concerning the location of the regions within the protein that confers the above-mentioned functional characteristics.

In two studies that addressed this deficit, chimeras were engineered to contain different proportions of two native isoforms that individually display markedly different kinetics. This led to the localization of a region that confers pH sensitivity (de la Horra et al., 2000) and a site that influences the apparent Na^+ affinity for type IIa cotransporters (de la Horra et al., 2001). Another approach, which does not rely on differentiating between functional properties of different isoforms for its success, is the substituted cysteine accessibility method (SCAM) (Akabas et al., 1992, 1994; Karlin and Akabas, 1998), in which cysteine residues are substituted by single point mutagenesis. These substitutions appear to be mostly well tolerated, as demonstrated by extensive cys-mutagenesis of *lac* permease protein (Kaback, 1997; Frillingos et al., 1998). If the substitution site is located in a functionally sensitive region and the cysteine residue is accessible from the aqueous environment, chemical modification of this residue by hydrophilic methanethiosulfonate (MTS) compounds can alter functional properties by increasing its effective size. Details of the method and underlying assumptions for SCAM are discussed in Karlin and Akabas (1998).

In our first use of SCAM applied to NaPi-IIa, we reported that externally applied MTS reagents do not affect the transport properties of the wild-type (WT) transporter, whereas one mutant (S460C) that had a novel cysteine introduced in the predicted third extracellular loop was found to be highly sensitive to impermeant MTS reagents (Lambert et al., 1999a). From our analysis of the kinetic properties before and after cysteine modification, we concluded that Ser-460 was most likely located in a region involved in reorientation of the empty carrier from outward- to inward-facing conformations. This study was the first to assign a functional role to a specific residue located in the putative third extracellular loop (ECL-3) of NaPi-IIa (see Fig. 1), and it encouraged us to investigate this part of the protein in more detail.

We now describe the results of applying SCAM to the region surrounding Ser-460 from Arg-437 through Leu-465 (see Fig. 1). First, we examined the effect of positively charged MTS reagents on the transport activity of the mutants. Based on the periodic sensitivity to 2-aminoethyl MTS hydrobromide (MTSEA) for mutants with substituted cysteines at sites before Ser-460, our findings were consistent with this stretch being membrane associated and folded as an α-helical motif. In contrast, mutants with substituted cysteines at sites after Pro-461 showed little MTS sensitivity. Second, we characterized the kinetic parameters of the functional mutants to assess the effect of cysteine mutagenesis on functional properties of the transporter. Whereas mutagenesis caused no significant change in apparent substrate activation properties, some mutants showed either significantly altered voltage and/or pH dependency as well as uncoupled slippage current, compared with the wild-type profile. In our revised topology of the ECL-3 region of NaPi-IIa, we postulate a re-entrant loop that incorporates the aforementioned α-helix together with sites that influence voltage and pH dependency of the transporter.

MATERIALS AND METHODS

Molecular Biology

Mutations were introduced following the QuickChange Site-directed Mutagenesis Kit manual (Stratagene). Briefly, 10 ng of the plasmid containing the rat NaPi-IIa cDNA were amplified with 2.5 U of Pfu DNA polymerase in the presence of 250 nM of primers. PCR amplification was performed with 20 cycles at 95°C (30 s), 55°C (1 min), and 68°C (12 min). Then, 10 U of DpnI were added directly to the amplification reaction and the sample was incubated for 1 h at 37°C to digest the parental, methylated DNA. XL1-blue supercompetent cells were transformed with 1 μl reaction mixture and plated onto LB-ampicillin-methicillin plates. The sequence was verified by sequencing (Microsynth). All constructs were cloned in pSport1 (GIBCO BRL). In vitro synthesis and capping of cRNA's were done by incubating the rat NaPi-IIa constructs, previously linearized by NotI digestion, in the presence of 40 U of T7 RNA polymerase (Promega) and Cap Analogue (NEB) (Werner et al., 1990).

Secondary structure predictions were made using the DNASIS software, v. 2.1 (Hitachi Software Engineering Ltd.)

Reagents and Solutions

All standard reagents were obtained from either Sigma-Aldrich or Fluka. MTS reagents were obtained from Toronto Research Chemicals.

The solution compositions (mM/liter) were as follows. (a) Oocyte incubation (modified Barth's solution): 88 NaCl, 1 KCl, 0.41 $CaCl_2$, 0.82 $MgSO_4$, 2.5 $NaHCO_3$, 2 $Ca(NO_3)$, 7.5 HEPES, adjusted to pH 7.6 with TRIS and supplemented with antibiotics (10 mg/liter gentomycin, streptomycin). (b) Control superfusate (ND100): 100 NaCl, 2 KCl, 1.8 $CaCl_2$, 1 $MgCl_2$, 5 HEPES, and adjusted to pH 7.4 with KOH. (c) Control superfusate (ND0): as for ND100, but with *N*-methyl-D-glucamine or choline chloride used to replace Na^+. Solutions were adjusted to pH 7.4 with HCl or KOH as required. Solutions with intermediate Na^+ concentrations were prepared by mixing ND0 and ND100 in the appropriate proportions. (d) Substrate test solutions: inorganic phosphate (P_i) was added to ND100 from 1 M K_2HPO_4 and KH_2PO_4 stocks that were mixed to give the required pH (7.4 or 6.2). Phosphonoformic acid (PFA) was added to the appropriate control superfusate from frozen stock (100 mM), and the pH was adjusted. PFA was obtained as a trisodium salt (Na^+) and the Na^+ concentrations were adjusted accordingly. (e) The MTS reagents MTSEA and 2-(triethylammonium)ethyl MTS bromide (MTSET) were prepared from dry stock in DMSO to give 1 M stock solutions. These were stored at −20°C until required and added to ND100 solution. The final concentration of DMSO did not exceed 0.1% and DMSO at this concentration was confirmed to not alter the kinetic characteristics of the expressed constructs.

Immunoblotting of Oocyte Homogenates-Western Blotting

Yolk-free homogenates were prepared 3 d after injection (H_2O or cRNA). Pools of five oocytes were lysed together with 100 μl of homogenization buffer [1% Elugent $C_{12}E_6$ (Calbiochem) in 100 mM NaCl, 20 mM Tris/HCl, pH 7.6], by pipetting the oocytes up and down (Turk et al., 1996). To pellet the yolk proteins, samples were centrifuged at 16,000 *g* for 3 min at 22°C. 10 μl of the supernatant in 2× loading buffer (4% SDS, 2 mM EDTA, 20% glycerol, 0.19 M Tris/HCl, pH 6.8, 2 mg/ml bromphenol blue) were separated on a SDS-PAGE gel and separated proteins were transferred to a nitrocellulose membrane (Schleicher & Schuell). The membrane was then processed according to standard procedures (Sambrook et al., 1989) using a rabbit polyclonal antibody raised against an NH_2-terminal synthetic peptide of the rat NaPi-IIa cotransporter. The specificity of the antibody has been demonstrated previously (Custer et al., 1994). Immunoreactive proteins were detected with a chemiluminescence system (Pierce Chemical Co.).

Functional Assays

Radiolabeled P_i Uptake. This procedure has been described in detail elsewhere (Werner et al., 1990). $^{32}P_i$ uptake was measured 3 d after injection in water injected (control) and cRNA injected oocytes ($n = 5$).

Electrophysiology and Data Analysis. The standard two-electrode voltage clamp technique was used as described previously (Forster et al., 1998). Oocytes were mounted in a small recording chamber (100 μl vol) and continuously superfused (5 ml/min) with test solutions pre-cooled to 20°C. Unless otherwise indicated, the steady-state response of an oocyte to P_i was always measured at a holding potential (V_h) = −50 mV in the presence of 100 mM Na^+. Data were acquired online using DATAC software and compatible hardware (Bertrand and Bader, 1986) and pClamp v. 8.0 and Digidata 1200A hardware (Axon Instruments, Inc.). Data were sampled at a rate that corresponded to more than twice the recording bandwidth. Recorded currents were prefiltered using an analogue eight pole low-pass Bessel filter (Frequency Devices) that was set to 20 or 500 Hz for steady-state or pre–steady-state recording, respectively. Data were analyzed using routines supplied with Clampfit v. 8 (Axon Instruments, Inc.) and/or Prism v. 3.2 software (Graphpad Software Inc.).

For the P_i-activation protocol, P_i-induced currents (I_{Pi}) were obtained by subtraction of the response in the ND100 control solution, without P_i. Dose response was determined from the responses to 0.01, 0.03, 0.1, 0.3, 1, and 3 mM P_i. (in ND100). For the Na^+-activation protocol, the dose response was determined from the responses to 1 mM P_i in 0, 10, 25, 50, 75, and 100 mM Na^+. I_{Pi} was measured relative to the control solution NDX, where X represents the Na^+ concentration (mM).

Using a nonlinear regression routine, the modified Hill equation was fit to the P_i or Na^+ dose response data:

$$I_{Pi} = I_{Pi}\max[S]^{n_H}/\left\{[S]^{n_H} + (K_m^s)^{n_H}\right\}, \quad (1)$$

where $[S]$ is the concentration of the variable substrate, I_{Pi}max is the extrapolated maximum current, K_m^s is the concentration of substrate S that gives a half maximum response or apparent affinity constant, and n_H is the Hill coefficient.

Current-voltage (I-V) curves were obtained by applying a series of voltage steps of 60-ms duration to the test potential from a standard holding potential (V_h) = −60 mV. The P_i-dependent currents were obtained by subtracting corresponding records from one another belonging to sets obtained in ND100 and ND100 + P_i (1 mM). This same voltage step protocol was used to obtain pre–steady-state relaxations (see Appendix), except that the low-pass filter setting was increased and more signal averaging was used where necessary.

To quantify altered steady-state charge distribution, we assumed that all intramembranous (pre–steady state) charge movements could be lumped into a single process described by the Boltzmann relation:

$$Q = Q_{hyp} + Q_{max}/\{1 + \exp[-ze(V - V_{0.5})/kT]\}, \quad (2)$$

where Q_{max} is the maximum charge translocated, Q_{hyp} is the steady-state charge at the hyperpolarizing limit and depends on V_h, $V_{0.5}$ is the voltage at which the charge is distributed equally between the two states, z is the apparent valency per cotransporter, e is the electronic charge, k is Boltzmann's constant, and T is the absolute temperature. Eq. 2 was fit to the data by nonlinear regression analysis. A single exponential function was fit to the pre–steady-state relaxations using a fitting algorithm based on the Chebychev transform supplied with pClamp v. 8. For some batches of oocytes, a linear baseline correction was applied to eliminate contamination from Ca^{2+}-activated Cl^- currents for voltage steps to $V \geq +40$ mV.

Incubation with MTS Reagents. Freshly prepared MTSEA/MTSET (see above) was delivered to the oocyte chamber using a stainless steel cannula (0.3 mm i.d.) positioned near the cell and fed by gravity. Reagents were always applied in the presence of ND100 at a holding potential $V_h = -50$ mV, unless otherwise indicated. Incubation was followed by a 1-min washout period before applying P_i (1 mM) as the test assay. Another 1-min washout period was allowed before reincubation at the next concentration of MTS reagent to ensure complete removal of substrate and return of response to a steady state. We routinely used cells that expressed the WT and S460C transporters as negative and positive controls, respectively, during each experimental session. Apparent second-order reaction rates for the Cys modification were determined by fitting a single exponential to the time or concentration dependency data after normalizing to the control response:

$$I(c) = \exp(-ctk), \quad (3)$$

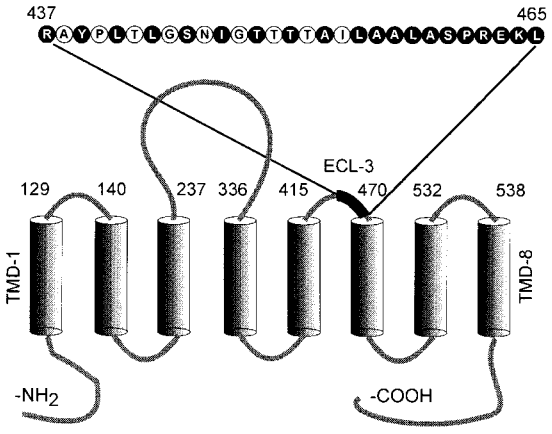

FIGURE 1. Topological representation of the type IIa Na^+/P_i cotransporter that shows the eight putative membrane-spanning domains (TMD-1 to -8) determined from hydropathy analysis. The amino acid residues in the stretch from site 437 through site 465 of the putative ECL-3 are shown expanded. Residues in this stretch that were mutated individually to cysteines are indicated by filled circles. Amino acids are named using the single letter code.

where $I(c)$ is the electrogenic response after incubation in MTS reagent at concentration c for t seconds, normalized to the control response, and k is the apparent second-order rate constant (Karlin and Akabas, 1998; Pascual and Karlin, 1998).

RESULTS

Protein Expression and Basic Function of Mutants

Fig. 1 presents a topological representation of the rat NaPi-IIa protein, with the location of the residues in the predicted ECL-3 that were mutated to cysteines. We injected *Xenopus laevis* oocytes with cRNA coding for each mutant. The cells were subsequently checked for protein expression by means of Western blot of the whole cell lysate (Fig. 2) and functional transport by using $^{32}P_i$ uptake and/or a basic electrophysiological assay (1 mM P_i, −50 mV holding potential, data not shown). In the latter assay, oocytes that responded to P_i with a reproducible inward current ≤ −20 nA were assumed to have expressed a functionally active mutant (Fig. 2, +) and other mutants were designated inactive (−). Before we concluded that a particular construct was indeed inactive, we repeated the injection procedure by using oocytes from at least one other donor frog and also repeated the cRNA synthesis. As a general rule, the P_i-induced currents for the mutant-expressing oocytes were usually less than those obtained from WT-expressing oocytes, and the absolute current levels depended on the oocyte batch. For all mutants that gave functional expression, we detected a main band in the Western blots, the position of which corresponded to the molecular weight of the WT rat NaPi-IIa cotransporter (70–90 kD). Taken together, these findings indicated that for the functional mutants, cysteine mutagenesis had not affected the basic transport function (Na^+-coupled P_i cotransport) and that these constructs were indistinguishable from the WT in terms of the expressed protein.

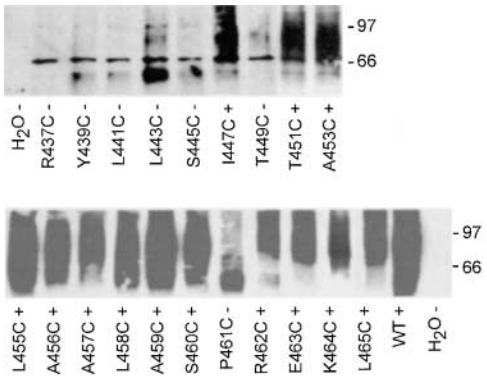

FIGURE 2. Protein expression and function of mutant cotransporters. Western blots of whole cell lysate from oocytes injected with cRNA coding for the indicated mutant constructs (see Fig. 1) as well as wild type (WT) and water injected (H_2O) oocytes as controls. The two Western blots were made from lysates using different batches of oocytes. The main band in the range 80–100 kD corresponds to the glycolsylated form of NaPi-IIa. The symbol after the name signifies whether functional activity was detected: +, cells displayed P_i-induced currents > −20 nA (V_h = −50 mV, P_i = 1mM); −, cells displayed neither electrogenic activity (< −20 nA) nor $^{32}P_i$ uptake above the background level.

Mutant P461C, which was inactive according to the above criteria, showed a lower molecular weight band at ~40–50 kD. This band most likely corresponds to the unglycosylated NaPi-IIa protein (Hayes et al., 1994). This was also the case for the mutants in the stretch R437C through T449C, with the exception of I447C, which was found functionally active. On the basis of these initial experiments ($^{32}P_i$ uptake and P_i-induced current; protein expression pattern), we concluded that cysteine substitutions at positions 437–446, 448, 449, and 461 led to critical structural alterations that were incompatible with correct synthesis of the fully glycosylated cotransporter protein, and thus led to a loss of apparent transport function.

Effect of MTSEA on Cotransport and Slippage Function

NaPi-IIa exhibits two modes of transport that involve translocation of substrate and net charge across the membrane: cotransport mode (Na^+/P_i-cotransport) and uncoupled leak mode (Na^+-slippage) (Forster et al., 1998; see also Fig. 6 A, below). The latter mode accounts for ~10% of the current evoked at saturating P_i and can be quantified by using the Na^+/P_i cotransport inhibitor PFA (Kempson, 1988) that also blocks the slippage mode current (Forster et al., 1998). To assess the effect of MTS reagents on transport function, both modes were considered as potential targets for functional modification.

We previously established that P_i transport of mutant S460C was fully abolished by pre-incubation in 100 μM of MTS reagents (MTSEA, MTSET, and MTS-ethylsulfonate) (Lambert et al., 1999a) for short time periods (<5 min). An examination of the response of the functionally active new mutants under these same incubation conditions indicated that full inhibition of P_i-induced electrogenic response (I_{Pi} at 1 mM, −50 mV) was not achieved in all cases. For incubation in 100 μM MTSEA (3-min incubation period), four mutants (A453C, A456C, A457C, and S460C) were fully inhibited, three mutants (L455C, L458C, and A459C) were partly inhibited (>20%), and six mutants (I447C, T451C, and R462C through L465C) showed little or no inhibition (<20%) (data not shown). Incomplete inhibition of cotransport function could indicate an intermediate condition in which the full loss of cotransport function, observed for S460C, had not yet been reached due to slower reaction rates of the MTS reagent with the cysteine in question; i.e., the apparent accessibility depended on the position of the cysteine. Alternatively, modification of the novel cysteine may have indeed occurred and this altered the kinetics (e.g., substrate af-

finity, turnover rate) to manifest itself as a partial inhibition of transport rate.[2] To distinguish between these two possibilities, we performed dose–response assays by incubating each oocyte in successively larger concentrations of MTSEA (see MATERIALS AND METHODS). Fig. 3 A shows representative recordings from oocytes that expressed the WT, S460C, and A453C in response to successive test applications of 1 mM P_i (I_{Pi}) and 3 mM PFA (I_{PFA}), initially and after incubation for 3 min in MTSEA at the concentrations indicated. As previously reported for the WT transporter, no significant alteration was observed in either I_{Pi} or I_{PFA} (Fig. 3 A, top), whereas for S460C the responses to PFA and P_i were the same after incubation in 1000 μM MTSEA (center). Moreover, we observed that the absolute holding current level reached during PFA application remained essentially unchanged during each experimental run. In contrast, for other mutants we observed a progressive increase in I_{PFA} when the concentration of MTSEA was increased, for mutant A453C (Fig. 3 A, bottom). However, like S460C, the absolute holding current reached during PFA application did not change throughout the recording period. For A453C, I_{Pi} became progressively smaller, eventually reversed in direction, and, after incubation in 1,000 μM MTSEA, it was equivalent to I_{PFA}. This behavior was also observed for L455C, whereas A456C, L458C, A457C, and A459C behaved like S460C, with no detectable change in the magnitude of I_{PFA} at −50 mV (data not shown). In all cases, the invariance of the absolute level reached during PFA application indicated that the MTSEA treatment had not affected the ability of PFA to fully block the slippage current. Moreover, the equivalence of I_{PFA} and I_{Pi} for most of the mutants after incubation in 1,000 μM MTSEA suggested that the MTSEA reaction had reached completion at this concentration; i.e., complete inhibition of the Na^+/P_i-cotransport function was achieved.

We established that the increased I_{PFA} after MTSEA treatment observed in the case of A453C was still a Na^+-dependent current (Na^+ slippage) by performing the assay at two Na^+ concentrations (100 and 50 mM), as shown in Fig. 3 B for another representative oocyte. When the superfusate changed from ND100 to ND50, there was a corresponding upward deflection of the holding current that was partly due to the leak component introduced by the exogenous protein and partly due to the endogenous response as seen for a noninjected oocytes from the same batch (Fig. 3 B, bottom).

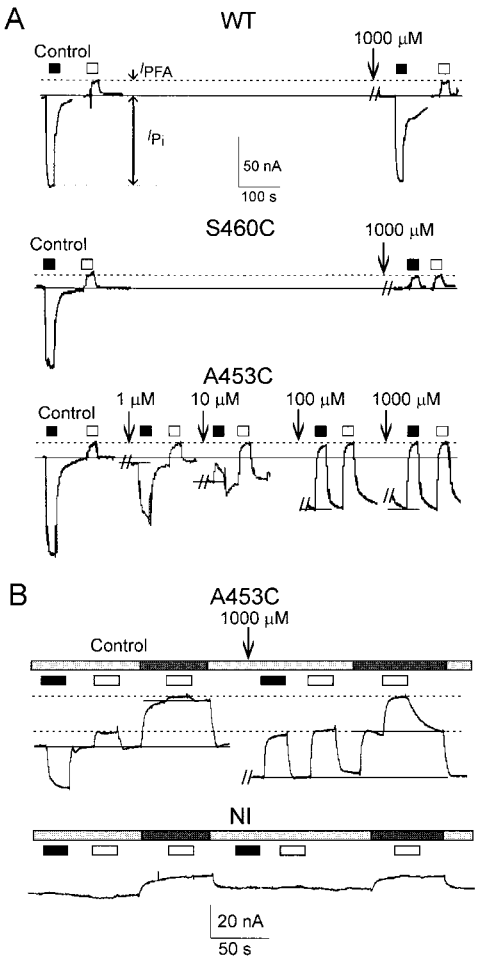

FIGURE 3. Effect on electrogenic response of incubation in MTS reagents. (A) Excerpts from continuous recordings made from representative oocytes that expressed the WT (top), S460C (center), and A453C (bottom) constructs, respectively. After a control application, substrates P_i (1 mM) (filled bars) and PFA (3 mM) (empty bars) were applied successively and tested after incubation (vertical arrows) in MTSEA for 3 min and washout at the concentration indicated. Only the baseline that immediately preceded application and washout of the test substrates is shown. The dashed line indicates holding current reached during control PFA application. Continuous line indicates initial holding current in ND100 superfusate. No external adjustment of current offset was made during the recording period. Cells were continuously voltage clamped to −50 mV during whole experiment; records were low-pass filtered at 20 Hz, sampling 2 ms/point. I_{PFA} and I_{Pi} are the changes in holding current induced by P_i and PFA, respectively, relative to the holding current in ND100. (B) Excerpts from two contiguous recordings that illustrate the effect of changing external Na^+ on slippage before and after MTSEA exposure to an oocyte that expressed A453C and a noninjected (NI) oocyte. The external solutions were changed as indicated: ND100 (light gray bars), ND50 (dark gray bars), P_i (1 mM) (filled bars), PFA (3 mM) (empty bars). Dotted lines indicate holding currents reached during PFA, continuous lines indicate current level in the absence of test substrate.

[2]A third possibility, that the number of active transporters in the membrane was partially reduced (for example, by the induction of endocytosis by the MTS reagent), could be rejected because we observed no change in membrane capacitance during the incubation period (data not shown). This would otherwise indicate a reduction of membrane area that normally accompanies endocytosis of NaPi-IIa (Forster et al., 1999b).

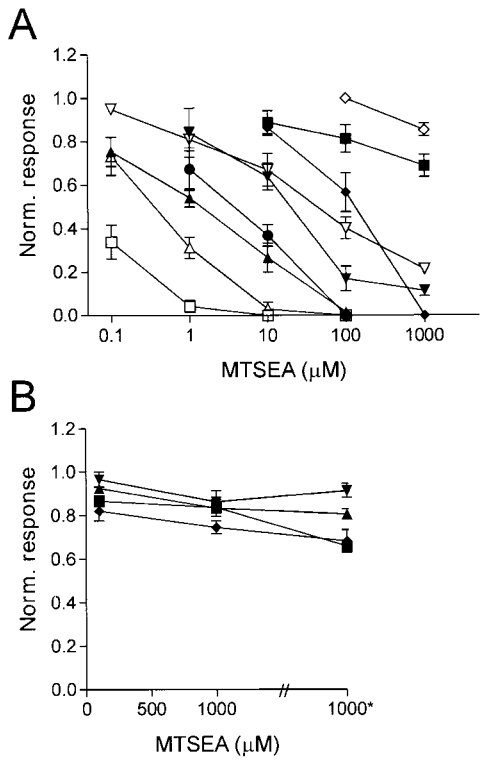

FIGURE 4. Effect of incubation in MTS reagents on the cotransport mode. Suppression of P_i-induced response was calculated by determining $I_{Pi} - I_{PFA}$ (indicated on WT record, Fig. 3 A) after each incubation and normalizing this to the initial control response. Each point represents mean ± SEM of at least four determinations using oocytes from two donor frogs. (A) Data for mutants with Cys substitution before Pro-461 tested at selected concentrations of MTSEA to determine the range of sensitivity: I447C (◇); T451C (■); A453C (●); L455C (◆); A456C (▲); A457C (□); L458C (▽); A459C (▼); S460C (△). (B) Data for mutants with Cys substitution after Pro-461 that were tested at only two MTSEA concentrations (100 and 1,000 μM). Each cell was also tested after a second incubation at 1,000 μM MTSEA under the same conditions (*). R462C (■); E463C (▲); K464C (▼); L465C (◆). Points have been joined for visualization purposes.

The holding current of the noninjected oocyte at V_h = −50 mV showed no significant changes in response to P_i and PFA either before or after MTSEA incubation, which indicated that the effects seen for the mutant were most likely specific properties of A453C. Moreover, for A453C, the near equivalence of the holding current levels reached during PFA application when superfusing with ND100 and ND50, before and after MTSEA treatment, strongly suggested that, in the latter case, PFA also blocked the MTSEA-modified Na^+-slippage current.

Quantification of the loss of P_i-induced activity (Na^+/P_i-cotransport function) was done by measuring the P_i-induced current relative to the PFA-induced holding current level at V_h = −50 mV (I_{Pi}-I_{PFA}). This procedure took account of the mutants that showed an increase in leak after MTSEA incubation, under the assumption that the slippage current remained uncoupled from the cotransport mode current. Mutants fell into two broad categories that depended on their sensitivity to MTSEA and the location relative to Pro-461, as revealed by a broad ranging assay that used MTSEA at concentrations spanning four orders of magnitude (Fig. 4 A). Mutants with substituted cysteines at sites before Pro-461 (with the exception of I447C and T451C) showed a progressive loss of P_i-induced activity for MTSEA concentrations ≤1,000 μM. Moreover, there were obvious differences in MTSEA sensitivities between these mutants. In contrast, mutants with novel cysteines at sites after Pro-461 showed a small but still measurable loss of function only after incubation in 1,000 μM MTSEA (Fig. 4 B). This increased slightly after repeated exposure at the same concentration, but could not be easily distinguished from a small rundown effect (<20%) previously reported for the WT cotransporter under repeated exposure to P_i (Forster et al., 1999b). Thus, for these mutants, either the substituted cysteine was not accessible by external MTSEA at 1,000 μM, or modification of the cysteine did not alter the Na^+/P_i cotransport function assayed.

To interpret our MTSEA sensitivity data in terms of the relative accessibility of particular Cys residues, we assumed that the MTS reagent accessed its reaction site from only one side of the membrane. It has been reported (Holmgren et al., 1996) that MTSEA is membrane permeant and could potentially access substituted or native cysteine residues from the intracellular side. Therefore, the observed difference in apparent accessibility might result from a lack of sidedness of MTSEA action or a mixture of effects. We have previously shown that in the case of S460C, modification of Cys-460 by externally applied MTS reagents results from external accessibility only (Lambert et al., 1999a). We checked that this was also the case for the other mutants by incubating representative cells expressing each functional mutant with the impermeant reagent MTSET and we obtained close to the same level of inhibition as for MTSEA at the same concentration (data not shown). Fig. 5 A, II, confirms the similarity of MTSEA and MTSET dose responses for S460C. These findings established that the MTSEA effects most likely resulted from external modification of the novel Cys residue.

If the MTSEA-Cys reaction is assumed to follow second-order reaction kinetics (Karlin and Akabas, 1998; Pascual and Karlin, 1998; see also Javitch, 1998; Kaplan et al., 2000), then the loss of cotransport function should be described by a single exponential decay (Eq. 3) from which the reaction rate (k) can be estimated. Either time of exposure (t) or concentration (c) can be used as independent parameters to determine k. We determined k using concentration as the independent variable over a limited range of MTS reagent concentration with a fixed 3-min exposure time, as shown in Fig. 5 A for all mutants

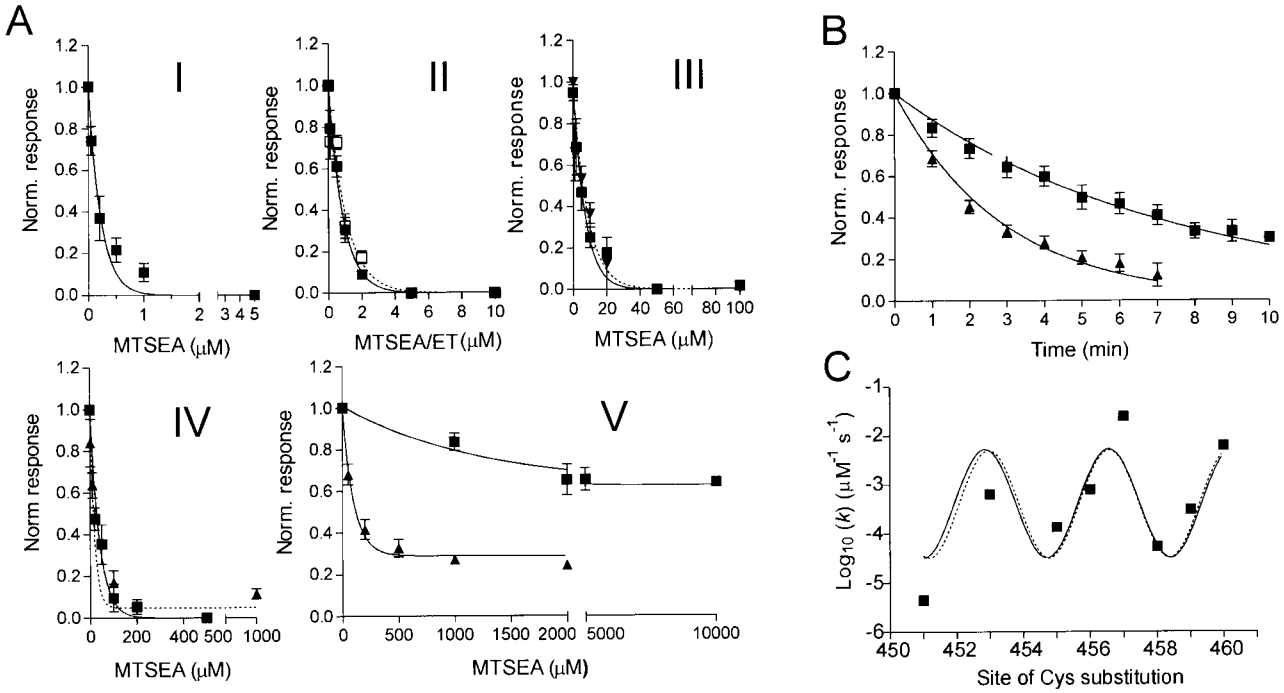

FIGURE 5. Determination of MTSEA-Cys reaction rates. (A) Loss of cotransport function for mutants T451C through S460C with MTSEA concentration as the independent variable. (I) A457C, (II) S460C (■, MTSEA; □, MTSET), (III) A453C (■) and A456C (▼), (IV) A455C (■) and A459C (▲), (V) L458C (▲) and T451C (■). Each data point represents mean from at least four cells. A single decaying exponential was fit to these data (Eq. 3). In II, the dotted line is a fit to the MTSET data. In IV, the dotted line is a fit to the A459C data. (B) The time dependency of the reaction of MTSEA with Cys-460 at 1 μM (■) and 5 μM (▲). Single decaying exponentials were fit to these data (continuous lines). Data points are mean ± SEM ($n = 5$) normalized to the initial response. When corrected for the MTSEA concentration, the apparent second-order reaction rate (k) was 2.2×10^{-3} μM^{-1} s^{-1} for 1 μM MTSEA and 1.3×10^{-3} μM^{-1} s^{-1} for 5 μM MTSEA. (C) Shows a plot of apparent second-order rate constant (k) for MTSEA inhibition of P_i-induced transport function for each of the functional mutants between T451C and S460C. Continuous line is an unconstrained sine-wave fit to the data points using a nonlinear regression algorithm. The dotted line is a sine-wave fit to the data points with its period constrained to 3.6 residues.

with novel cysteines substituted before Pro-461 (except I447C). Most mutants showed a well-behaved decay to zero, with the notable exceptions of L458C and T451C, which decayed to plateaus around 20 and 70%, respectively, of the original cotransport activity (Fig. 5 A, V). The range of rate constants (k) derived from fitting Eq. 3, with $t = 180$ s, varied from 2.5×10^4 s^{-1} M^{-1} (A457C; Fig. 5 A, I) to 4.5 s^{-1} M^{-1} (T451C; Fig. 5 A, V). In addition, we confirmed for the S460C mutant that at a given concentration of MTSEA, the loss of cotransport function also depended on the cumulative time of exposure in an exponential manner for two fixed concentrations of MTSEA (1 and 5 μM). Like the concentration dependence data, these data could be described by a single exponential decay. The ratio of the two exponents estimated from the fits ≈3, which is close to the ratio of the nominal test concentrations used, as would be expected from Eq. 3. Furthermore, k estimated from the fit at 1 μM MTSEA (2.2×10^{-3} μM^{-1} s^{-1}) is in the same range as that obtained from the fit to concentration dependency data (4.2×10^{-3} μM^{-1} s^{-1}). The difference would not result in a significant difference in the calculated k, when expressed logarithmically (see below).

The estimates of k obtained from the fits in Fig. 5 A could be best plotted logarithmically as a function of mutation site, as shown in C. The wide variation in reaction rates indicated that there was a location-dependent accessibility of the substituted cysteine residue by MTSEA. Moreover, the pattern suggested that accessibility varied periodically with a period between three and four residues spacing, as indicated by a free sine wave fit.

Kinetic Properties of Functional Mutants

In addition to the above SCAM experiments, the Cys mutations per se might produce alterations that provide information on the functional importance of given amino acid residues (or regions) within the transporter molecule. Therefore, we further characterized the functional mutants using previously established electrophysiological assays and the data were compared with the standard "fingerprints" for type II Na^+/P_i cotransport; namely, Michaelis-Menten P_i-activation, cooperative Na^+ activation, slippage, pH dependency, and steady-state and pre–steady-state voltage dependency (Forster et al., 1998). For each functional assay, one or two representa-

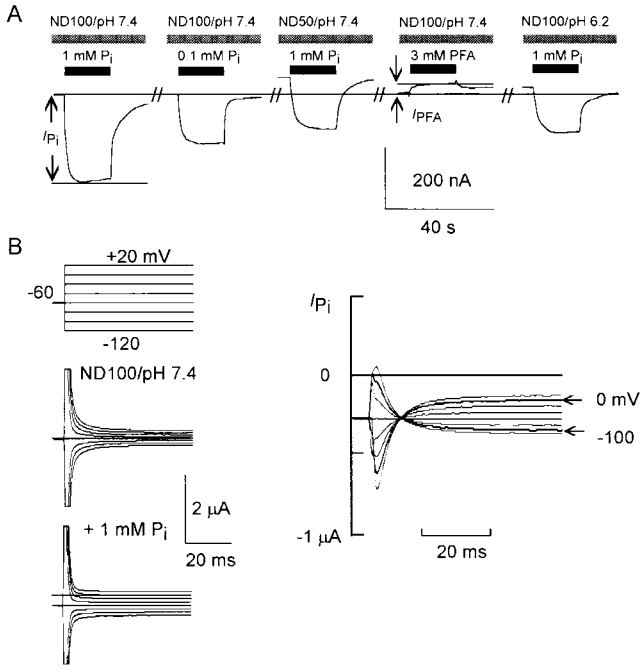

FIGURE 6. Steady-state functional assay of electrogenic properties. (A) Current records from a representative oocyte that expressed the WT protein measured under voltage-clamp conditions (V_h = −50 mV). Different substrate combinations were applied in the sequence during the time indicated by the bars to allow quantification in terms of P_i and Na^+ activation ($I_{Pi}^{0.1P_i}/I_{Pi}^{1.0P_i}$ and $I_{Pi}^{50Na}/I_{Pi}^{100Na}$, respectively), and slippage [$I_{PFA}/(I_{PFA} - I_{Pi})$] and pH ($I_{Pi}^{pH6.2}/I_{Pi}^{pH7.4}$). All data are shown relative to the same initial baseline level (continuous line) that was stable throughout the assay (ND100, pH 7.4). Test substrates were applied for ~20 s, as indicated. The speed of response to changing substrate conditions depended on the oocyte batch and also reflects diffusion limitations of the unstirred layer surrounding the oocyte, particularly for that part of the cell exposed to the base of the chamber (Forster et al., 1998, 2000). After substrate washout, the holding current was always allowed to return to the same baseline before the next application. The shift in baseline current for a 50% reduction in external Na^+ (ND100 to ND50) is contributed by the slippage current response and the endogenous oocyte response. The change observed for a decrease in pH of ND100 (pH 7.4 to 6.2) is an endogenous response also reported for noninjected oocytes (Forster et al. 2000). (B) Derivation of the steady-state voltage dependency. (Left) Current response to voltage steps from V_h = −60 mV to potentials in the range −120 to +20 mV in ND100 (top) and ND100 +1 mM P_i (bottom). Note the downward shift in holding current at −60 mV caused by the application of P_i. (Right) The difference between two sets of traces gives the P_i-dependent current (I_{Pi}). Responses at V = −100 and 0 mV used for the data Fig. 7 C (arrow). The nonlinear relaxations to the steady state arise from pre–steady-state charge movements (see APPENDIX).

tive oocytes that expressed the WT protein from the same donor frog were routinely used as a control to confirm reproducibility of the WT behavior. Representative records of the assays for a typical WT-expressing oocyte are shown in Fig. 6.

Steady-state Substrate Activation. A complete dose response with respect to P_i or Na^+ was not possible in all cases because the P_i-induced current at lower substrate concentrations could not be separated reliably from endogenous effects.[3] Therefore, for the purpose of screening for any changes in P_i activation kinetics, we determined the ratio of current induced by 0.1 mM P_i ($I_{Pi}^{0.1P_i}$) [close to the WT apparent affinity for P_i ($K_m^{P_i}$); Forster et al., 1998] and 1.0 mM P_I ($I_{Pi}^{1.0P_i}$) (Fig. 6 A). Similarly, for Na^+ activation, we compared the current at 50 (I_{Pi}^{50Na}) and 100 (I_{Pi}^{100Na}) mM Na^+ at near saturating P_i (1 mM P_I, V_h = −50 mV) as an indicator of shifts in the apparent Na^+ affinity (K_m^{Na}) (Fig. 6 A). None of the active mutants gave large deviations of the respective "activation indices" $I_p^{0.1P_i}/I_p^{1.0P_i}$ and $I_{Pi}^{50Na}/I_{Pi}^{100Na}$ from the WT range (Fig. 7 A). From these data and the complete dose–response data,[3] we concluded that the apparent substrate affinities and the implied substrate stoichiometries were minimally affected by the Cys mutagenesis.

Slippage. We assayed the slippage properties of functional mutants by comparing I_{Pi} (1 mM P_i) and I_{PFA} (3 mM PFA) at V_h = −50 mV, measured relative to the baseline holding current (Fig. 6 A). The slippage was quantitated as a fraction of the total electrogenic cotransport mode activity [$I_{PFA}/(I_{PFA} - I_{Pi})$]. Here, we assumed that in the presence of near saturating P_i (1 mM), the occupancy of conformational states that contribute to the slippage mode only is zero; i.e., the leak current is uncoupled from the cotransport current. The relative slippage index [$I_{PFA}/(I_{PFA} - I_{Pi})$] (Fig. 7 B) lay within the range observed for the WT, with the exception of mutants A453C, L455C, and A459C, which showed slightly larger indices compared with the WT. In the present study, we did not pursue the characterization of this property further because, in the case of several low-expressing mutants, contamination from an endogenous response to PFA (e.g., Forster et al., 2000) would have significantly affected the accuracy of the data. Nevertheless, these findings suggested that some of the native residues in the putative ECL-3 are contributing to the slippage pathway kinetics. This is also in agreement with our previous study that characterized in detail the mutant S460C (Lambert et al., 1999a).

pH Sensitivity. A hallmark of type IIa Na^+/P_i cotransport is its pH dependency, whereby acidification of the extracellular medium results in suppression of transport. A reduction of pH from 7.4 to 6.2 has been previously reported to result in a 50–80% reduction in I_{Pi} at constant total P_i (Busch et al., 1994, 1995; Forster et al.,

[3]Michaelian responses (Eq. 1 with n_H = 1.0) were obtained for nine mutants for which we determined P_i activation curves (Fig. 7 A, *), with K_m^{Pi} ranging from 0.050 ± 0.001 to 0.12 ± 0.03 mM (n = 4), compared with 0.06 mM previously reported for the WT (Forster et al., 1998). For six mutants (Fig. 7 A, **) the Na^+ activation data yielded K_m^{Na} estimates in the range 44 ± 7 to 98 ± 21 mM (n = 4), compared with 52 mM for the WT (Forster et al., 1998) and with Hill coefficients that were all significantly >2 (compare n_H^{Na} = 2.9 for the WT, Forster et al., 1998).

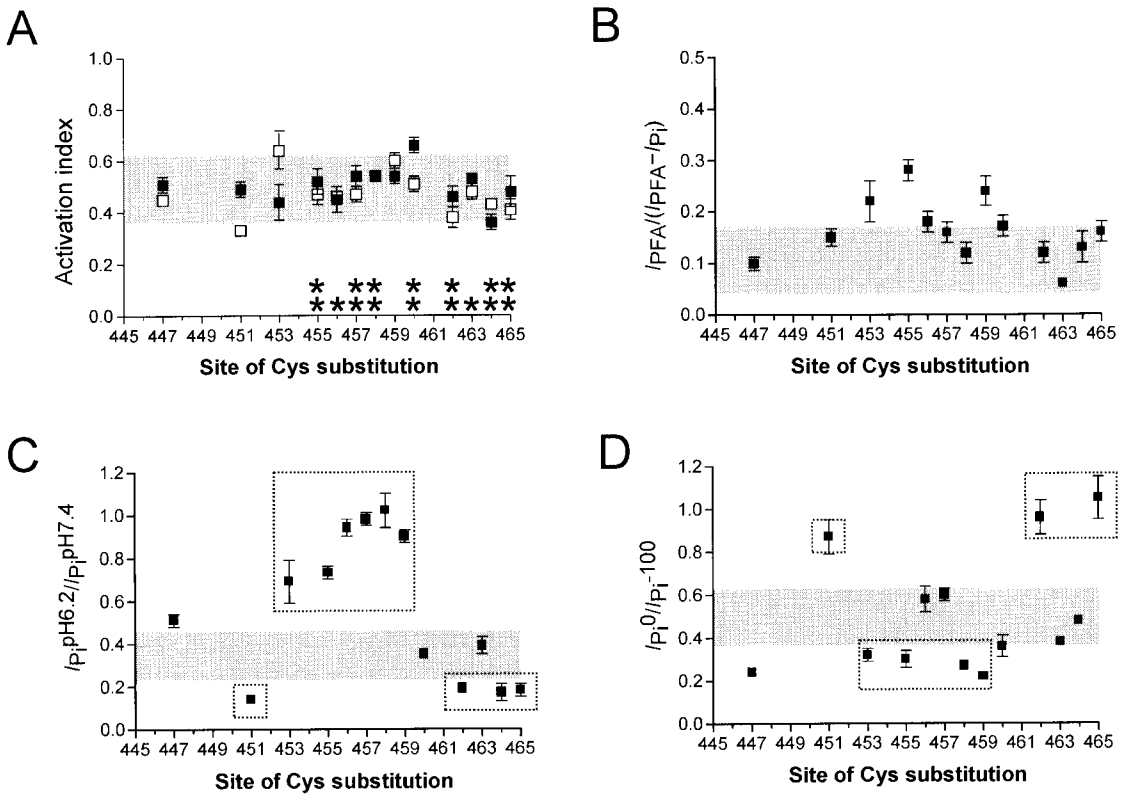

FIGURE 7. Overview of electrogenic properties of mutants. The shaded region in each case represents the typical range of values obtained for WT-expressing oocytes (mean ± 2 SEM) ($n \geq 4$, and assay repeated using oocytes from at least two donor frogs). (A) Substrate activation index at $V_h = -50$ mV for P_i ($I_p^{0.1P_i}/I_p^{1.0P_i}$) (■) and Na^+ ($I_{Pi}^{50Na}/I_{Pi}^{100Na}$) (□). *Mutants for which a complete P_i dose response was obtained. **Mutants for which a complete Na^+ dose response was also obtained. (B) Uncoupled leakage current, or slippage for each active mutant, expressed as a fraction of the total cotransport current at $V_h = -50$ mV). (C) The pH dependency of the mutants at $V_h = -50$ mV. For each oocyte, the ratio of the current induced at pH 6.2 to that at 7.4 ($I_p^{6.2}/I_p^{7.4}$) was determined (1 mM total P_i, $V_h = -50$ mV, ND100) and data pooled as in A. (D) Voltage dependence of the mutants. For each oocyte, the ratio of the current induced at $V_h = 0$ to that at $V_h = -100$ mV (I_p^0/I_p^{-100}) was determined (1 mM P_i, 100 mM Na^+) and data pooled as in A. Points without error bars have SEM smaller than the symbol. Boxed points in C and D indicate sites where Cys mutagenesis results in reciprocal deviations from the WT phenotype (see DISCUSSION).

1998, 2000). For assessing the effect of the Cys mutagenesis on pH sensitivity, we determined the electrogenic response at pH 7.4 ($I_{Pi}^{pH7.4}$) and pH 6.2 ($I_{Pi}^{pH6.2}$) (with 1 mM total P_i, 100 mM Na^+, and $V_h = -50$ mV) (Fig. 6 A) and compared the ratio $I_{Pi}^{pH6.2}/I_{Pi}^{pH7.4}$ with that for the WT. Several mutants showed clear deviations from WT behavior (Fig. 7 C). For example, mutants A453C through A459C displayed significantly reduced sensitivity to pH, whereas some of the flanking mutants (T451C, R462C, K464C, and L465C) showed somewhat greater sensitivity compared with the WT.

Voltage dependency. Type IIa Na^+/P_i electrogenic behavior is characterized by the voltage dependency of I_{Pi}. The typical steady-state current–voltage relationship for the WT at near-saturating P_i (1 mM) and maximum usable external Na^+ (100 mM) is reasonably linear in the physiological range of potentials (-100 mV $< V < 0$ mV). Outside this range, we have previously reported evidence of saturating behavior (Forster et al., 1998). Moreover, I_{Pi} at 0 mV (I_{Pi}^0) is typically ~50% of the current evoked at -100 mV (I_{Pi}^{-100}) (Forster et al., 1998). To facilitate comparison of the I-V data for the mutants, we determined the ratio I_{Pi}^0/I_{Pi}^{-100} under standard conditions (1 mM P_i, 100 mM Na^+) by subtracting corresponding voltage jump records to determine I_{Pi} at the two test potentials (Fig. 6 B). As summarized Fig. 7 D, there was a scatter of I_{Pi}^0/I_{Pi}^{-100} values around that of the WT. Mutants I447C, A453C, L455C, L458C, and A459C had smaller I_{Pi}^0/I_{Pi}^{-100} ratios (i.e., greater voltage dependence), whereas mutants T451C, R462C, and L465C had I_{Pi}^0/I_{Pi}^{-100} ratios closer to unity (i.e., loss of voltage dependence).

The differences in I_{Pi}^0/I_{Pi}^{-100} ratios are conveniently visualized from the full I-V curves (see MATERIALS AND METHODS) over the voltage range –120 mV $\leq V \leq$ +20 mV, as shown in Fig. 8. Based on the shape of the I-V curves, we could assign each mutant to one of three categories: those having an I-V curve like the WT (Fig. 8 A), those showing a stronger voltage dependence (B),

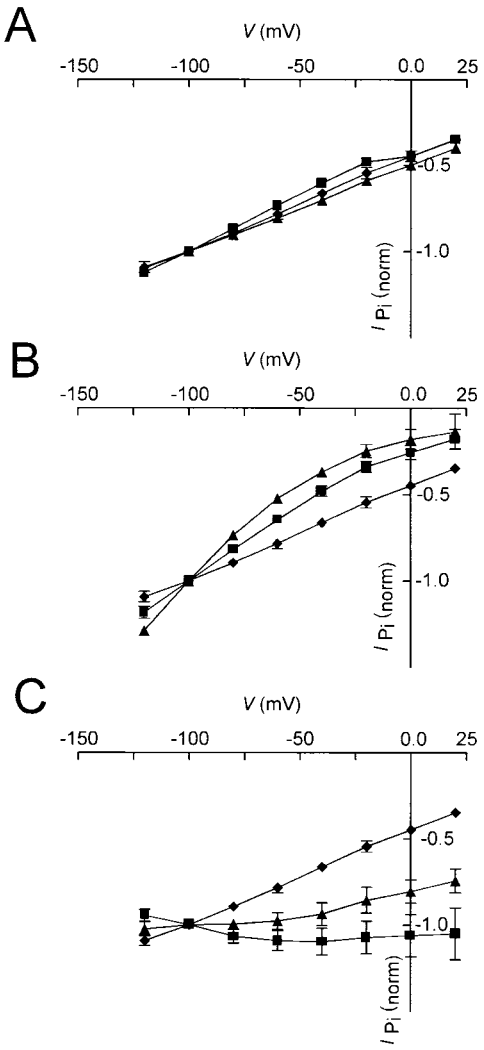

FIGURE 8. Current voltage curves for representative mutants belonging to the three categories referred to in the text. (A) E463C (■) and K464C (▲) that show an I-V similar to the WT; (B) I447C (■) and A459C (▲) that show supralinear I-V relations; (C) T451C (▲) and R462C (■) that show reduced voltage dependence. Points at each test potential were determined from voltage-step protocols in which the response to 1 mM P_i ND100 was subtracted from the response in ND100 alone. Data for each oocyte were then normalized to the current at −100 mV and pooled. Points without error bars have SEM smaller than the symbol. The same data set for WT (◆) is repeated in all cases. Continuous lines are for visualization only.

and those that showed a weaker voltage dependence (C) compared with WT.

In addition to the above steady-state analysis, performed on all functional mutants, pre–steady-state charge movements were also characterized for selected mutants with sufficiently high expression ($I_{Pi} \geq -60$ nA at P_i = 1 mM, V_h = −50 mV) (see APPENDIX). Pre–steady-state relaxations can provide additional information relating to voltage-dependent steps for Na^+-driven cotransport systems, which includes an estimate of the apparent valency (z) (Loo et al., 1993; Forster et al., 1998). In general, the alterations in voltage dependence seen in the steady state were reflected as corresponding shifts in the voltage dependence of the charge distribution (Q-V) and relaxation rate (τ-V) data (see Fig. A1, below). Moreover, we found that the apparent valency (z) for the mutants was not significantly altered from the WT estimate (see Table AI, below). This result suggested that the Cys mutagenesis had modified the kinetics of, but not removed, charges associated with the intrinsic voltage-dependent transitions of the transport cycle.

DISCUSSION

SCAM has been widely applied as a tool for structure–function studies of membrane transport proteins expressed in prokaryotic (e.g., Frillingos et al., 1998; Kaback 1997), eukaryotic (e.g., Akabas et al., 1992, 1994; Karlin and Akabas, 1998; Lo and Silverman, 1998a,b; Loo et al., 1998; Pascual and Karlin, 1998; Seal and Amara, 1998) preparations and in reconstituted membrane systems (e.g., Kaplan et al., 2000). This present work extends our previous cysteine scanning study of the type IIa Na^+/P_i cotransporter expressed in *Xenopus laevis* oocytes (Lambert et al., 1999a).

Of the 17 new mutants constructed in this study, 11 were functionally active as confirmed by $^{32}P_i$ uptake and/or electrophysiological assays. Moreover, Western blots of the functional mutants all showed a main band (80–90 kD) at the expected position for the fully functional and glycosylated WT NaPi-IIa protein (Hayes et al., 1994). This established that the Cys mutagenesis had not resulted in significant changes to the protein expression pattern. Nonfunctional mutants, on the other hand, did not show the expected 80–90-kD band. For these mutants, there was evidence of the presence of the core glycosylated NaPi-IIa protein. In our hands, using the oocyte expression system, these particular constructs could not be stably expressed as the fully glycosylated form. That cysteine substitutions are generally well tolerated is evidenced by the success obtained with SCAM applied to a number of transporters expressed in *Escherichia coli*, (e.g., Kaback, 1997; Frillingos et al., 1998; Mordoch et al., 1999; Iwaki et al., 2000). Our inability to obtain functional expression of all mutants may either reflect differences in the two expression systems or indicate the critical importance of the particular native residues in rendering proper synthesis/processing and/or stable expression of the NaPi-IIa protein.

Functional Implications of MTS Accessibility Pattern

Given that all expressed mutants had a WT-like cotransport mode (substrate activation; Fig. 7 A) meant that any changes in this function after MTS treatment

would support the respective Cys residue being: (a) at a site accessible to the MTS reagents via the aqueous milieu and (b) associated with the transport pathway. We found clear differences in the loss of cotransport mode function among the mutants with respect to MTSEA concentration, and there was an obvious demarcation of MTSEA effects at Pro-461. For mutants with Cys substitutions before this site, a site-dependent sensitivity to MTSEA was observed, whereas mutants after this site showed little sensitivity to MTSEA. This suggests that despite their functional involvement, the latter sites were only poorly accessible by either MTSEA or MTSET, or that Cys modification has no functional consequences. In contrast, at sufficiently high concentrations, complete or near complete inhibition of cotransport occurred for all members of the former group, with the exception of T451C. This suggests that these residues might constitute a common functional unit of the transport protein.

That PFA blocked the slippage mode for each mutant after MTSEA incubation implied that Na^+ was still able to bind to the empty carrier and the uncoupled leak pathway was intact. Moreover, the equivalence of the P_i and PFA responses indicated that both substrates were also able to bind to the protein. Our finding that modification of the engineered Cys residues from 451 through 460 led to complete or near complete inhibition of P_i-induced transport at sufficiently high MTSEA concentrations suggested that, after P_i binding, this stretch of amino acids plays a critical role in the translocation of the fully loaded carrier. Moreover, two mutants (A453C and L455C) showed greatly increased slippage current after MTSEA treatment, which suggested that modification of these sites had increased the turnover in the slippage mode. Similar behavior has been reported after treatment of the WT form of GAT1 with MTSET (Yu et al., 1998).

Kinetic Properties of Cys Mutants Confirm Functional Importance of ECL-3

In contrast to the WT-like P_i and Na^+ activation indices documented for all functional mutants (Fig. 7 A), the kinetic assays revealed that the Cys substitutions per se led to deviations from WT behavior for uncoupled slippage, pH and voltage dependence, with significantly altered kinetics in the case of the latter two phenotypes. That some constructs showed no significant alteration in one or more of these phenotypes suggested that we had detected functional "hot spots" and that the deviations from WT behavior were not simply a nonspecific outcome of the Cys mutagenesis.

Comparison of the pH and voltage-dependence profiles suggested a reciprocity of the deviations from WT behavior for these two phenotypes (see boxed data points in Fig. 7, C and D). For example, of the six mutants with Cys residues at adjacent sites from 453 through 459, four also displayed increased voltage dependence. Conversely, Cys substitution at the flanking sites 451 and 462–465 resulted in mutants with increased pH sensitivity that was matched by reduced steady-state voltage dependence. Such an interplay between pH and voltage dependence would not be unexpected based on the behavior of the WT cotransporter, whereby external acidification leads to a positive shift in the Q-V relation for the empty carrier-intrinsic charge distribution and a concomitant flattening of the steady-state I-V curves (Forster et al., 2000). The altered pH sensitivity observed for mutants with Cys substitutions after Pro-461 is also consistent with the recent finding that the REK motif (sites 462–464) of the mouse NaPi-IIa isoform is a determinant of pH dependency (de La Horra et al., 2000).

Of the three mutants that displayed significant reductions in steady-state voltage dependence, only one (R462C) involved the removal of a charged residue. This mutant also displayed altered pre–steady-state kinetics with a reduced relaxation time constant compared with the WT and a positive shift of the Q-V curve (see APPENDIX). This suggests that this residue plays a significant role in determining the electrogenic behavior and, by implication, interacts with the transmembrane electric field. The specificity of the involvement of Arg-462 is indicated by our finding that removal of nearby positive and negative charges (mutants K464C and E463C, respectively) did not alter the voltage dependence of I_{Pi}. For I447C, L458C, and A459C, we observed significant negative shifts in the Q-V and τ-V data, which correlated with the supralinear steady-state I-V curves. In contrast to the documented shifts in voltage dependence, the apparent valency (z) predicted from the Boltzmann fit was relatively insensitive to the mutagenesis (see Table AI). This parameter is most likely a weighted average of many charges, including those intrinsic to the transporter itself, as well as the movement of Na^+ to its binding site (Forster et al., 1998). Although a change in one or both components might be masked by the averaging effects, the constancy of z strongly suggests that the mutagenesis neither removed nor neutralized intrinsic charges associated with the empty carrier conformational changes. The effects of Cys mutagenesis on voltage dependence might then be attributed to shifts in the steady-state distribution of intrinsic charges. Moreover, the invariance of z would suggest that the charge at site 462 does not contribute to the intrinsic carrier charge movements per se, but could, for example, exert an electrostatic influence on other mobile charges that are directly involved in conformational changes. Significant alterations in electrogenic kinetics of the sodium glucose cotransporter, SGLT-1, have also been reported by Lo

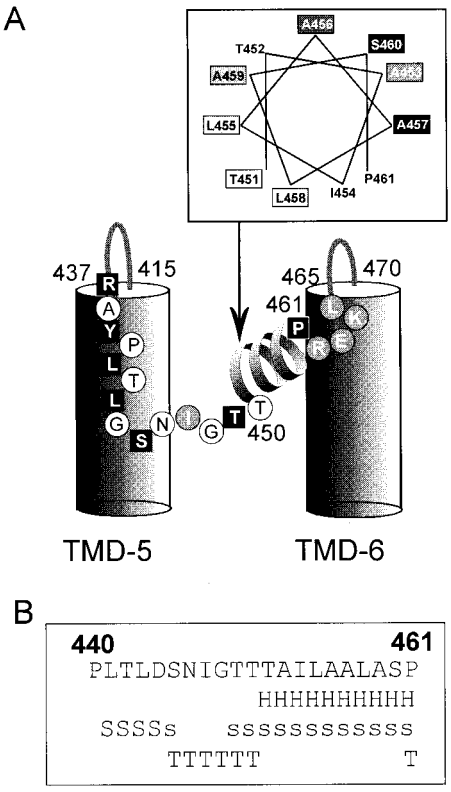

FIGURE 9. Interpretation of MTSEA accessibility in terms of an α-helix motif and its incorporation in a revised topology of NaPi-IIa. (A) The revised topology of ECL-3 depicted as a re-entrant loop, accessible to the extracellular medium and incorporating a 2.5 turn α-helix from Pro-461 to Thr-451. (Bold) Residues mutated to cysteines, (filled squares) nonfunctional mutants, (gray circles) functional mutants that showed little MTSEA sensitivity. The inset shows a helical wheel representation of the residues Pro-461 through Thr-451 with shading to represent their relative accessibility to MTSEA, based on the data in Fig. 5 C. (B) Predictions for secondary topology based on the Chou-Fasman algorithm for the region from Pro-440 through Pro-461. Upper and lower case letters indicate probable and possible predictions, respectively (S/s, sheet; H/h, helix; T, turn).

and Silverman (1998a,b) when a cysteine was substituted for a native alanine residue.

In summary, the region surrounding Ser-460 is involved in conferring slippage properties, voltage dependence, and pH dependence, but does not contain residues critical for defining apparent substrate affinities, at least when they are replaced by a cysteine. An understanding of the role these sites play in conferring pH and voltage dependence will require a detailed mutagenesis study.

A Revised Topology for ECL-3 Based on the Cys Accessibility Pattern

Our data prompted a revision of the existing topology for NaPi-IIa in the region of the previously predicted third extracellular loop, as depicted in Fig. 9 A. Part of this loop is depicted as re-entrant and is postulated to contribute to the transport pathway. The most novel feature of this topology is the proposed 2.5-turn α-helical motif from Pro-461 to Thr-451 (see inset for a helical wheel representation). Evidence for this motif is based on our finding of a periodic pattern (period 3.6 residues/turns) for the apparent rate constant of the MTSEA-Cys reaction for cysteines substituted between Ser-460 and Thr-451 (Fig. 5 C). This predicted motif is also supported by the secondary structure predictions obtained from the Chou-Fasman algorithm applied to the primary amino acid sequence for the type IIa Na^+/P_i cotransporter (Fig. 9 B).

We propose that Pro-461 performs a helix terminating and stabilizing role for the α-helix motif. The orientation of the helix and its position relative to the adjoining putative transmembrane domains (TMDs) is not possible to define from our present data. However from the MTSEA accessibility results, we assume that the most accessible residues form a face readily accessible to the aqueous medium. Moreover, our finding that Cys modification of two of the residues within the α-helix altered the slippage current suggests that this motif might lie within the uncoupled Na^+-slippage pathway. A further feature of the revised topology is the placement of Arg-462 within the transmembrane region because substitution of the native arginine for a neutral cysteine strongly influenced the voltage dependency of the transporter.

Reentrant loops have been proposed to establish the selectivity filter in ion channels (MacKinnon, 1995) and recent structure studies on the K^+ channel (Doyle et al., 1998) and aquaporin-1 (Murata et al., 2000) predict that these loops also contain short α-helical motifs. Based on their cysteine accessibility, Silverman (2000) has also proposed that some residues in the loop between TMD-4 and TMD-5 of SGLT-1 form an α-helix and contribute to the Na^+ binding and voltage sensing. Moreover, putative reentrant loops have been identified in the revised topologies of transport proteins such as the excitatory amino acid transporters (Seal and Amara, 1998; Yu et al., 1998; Grunewald and Kanner, 2000) and the human Na^+/H^+ exchanger (NHE1) (Wakabayashi et al., 2000), where they are postulated to form ion transport pathways.

APPENDIX

The current kinetic scheme for type IIa Na^+/P_i cotransport predicts that the voltage dependence of type IIa Na^+/P_i cotransport is conferred by the voltage dependent kinetics of the empty carrier and the first Na^+ binding (Forster et al., 1998). Here we show for selected mutants that the altered steady-state voltage depen-

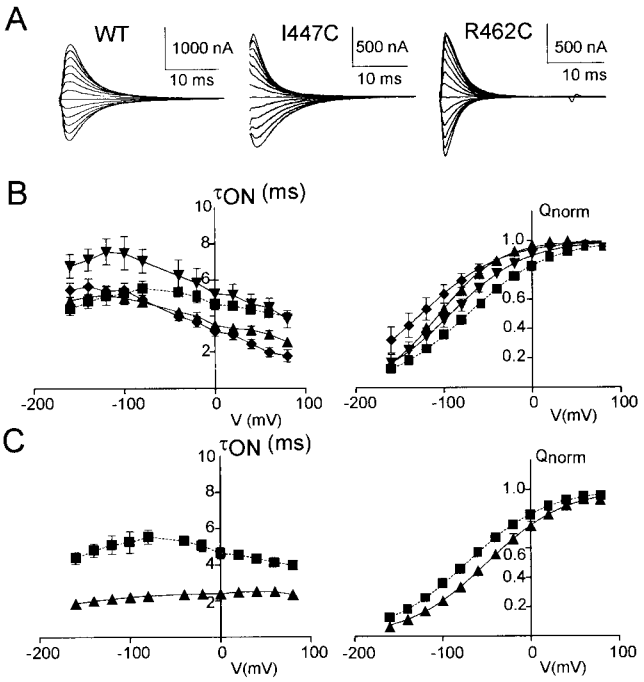

FIGURE A1. Properties of pre–steady-state relaxations for selected mutant constructs. (A) Typical pre–steady-state ON relaxations after subtraction of response in 3 mM PFA to eliminate endogenous components for the wild type (WT) and two mutants that deviate from WT behavior (I447C and R462C). Each data set is for voltage steps from −160 to +80 mV from V_h = −60 mV. Each trace is the average of four sweeps, low-pass filtered at 500 Hz. (B) τ_{ON} vs. V (left) and Q vs. V (right) data for mutants I447C (▲), L458C (▼), and A459C (◆) that show shifts toward hyperpolarizing potentials compared with the WT (■). C, τ_{ON} vs. V (left) and Q vs. V (right) data for mutant R462C (▲) that shows significantly faster relaxations and a shift toward depolarizing potentials compared with the WT (■). For the τ_{ON} vs. V data, a single exponential function was fit to ON relaxations. Data points are joined for visualization only. For the Q vs. V data, the same relaxations were integrated for both the ON and OFF (data not shown) transitions and the mean charge transfer was determined. Data were normalized and pooled as described in the APPENDIX. Lines are the result of fitting Eq. 2 to the pooled data: WT (broken), mutant (continuous).

dency is reflected in modified kinetics of the pre–steady-state charge movements induced by voltage steps.

For all the mutants examined, the addition of PFA (3 mM) to the ND100 solution led to a suppression of the relaxations seen with ND100 alone as previously reported for the WT (Forster et al., 1998, 2000). To analyze the relaxations, the PFA response (ND100 + PFA) was subtracted from the response in ND100 to eliminate endogenous currents. Fig. A1 (A) shows typical recordings for WT, I447C, and R462C after PFA subtraction. Differences between kinetics of WT and the two mutants are clearly seen. To account for different expression levels, a single Boltzmann function (Eq. 2) was first fit to the Q-V data for each oocyte, the data were then offset by the predicted Q_{hyp} and finally normalized to Q_{max}. The Boltzmann fit parameters for the pooled data (n = 6) are summarized in Table AI. Deviations of the Q-V data from the WT profile correlated qualitatively with those seen for the τ-V plots, whereby the direction of shifts in the midpoint potential of the charge distributions was the same as that for the peak of the τ-V data. For example, mutants I447C, L458C, and A459C all showed hyperpolarizing shifts (Fig. A1, B). This behavior correlated with the supralinear steady-state I-V curves documented for two of these mutants (Fig. 8 B). Mutant R462C, which was weakly voltage dependent in the steady state (Fig. 8 C) showed significantly faster relaxation time constants and evidence of a peak shifted toward depolarizing potentials (Fig. A1, C).

TABLE AI

Pre–steady-state Q-V Parameters for WT and Selected Mutants

NaPi-IIa construct	$V_{0.5}$*	z[1]
	mV	
WT	−72 ± 1	0.57 ± 0.01
I447C	−105 ± 1	0.75 ± 0.03
L458C	−93 ± 2	0.61 ± 0.03
A459C	−126 ± 4	0.57 ± 0.04
R462C	−50 ± 1	0.58 ± 0.02

*Parameters obtained from fit of Eq. 2 to normalized, pooled Q-V data. Fit parameters given as mean ± SEM of fit.

This work was supported by grants to H. Murer from the Swiss National Science Foundation (31-46523), the Hartmann Müller-Stiftung, the Olgar Mayenfisch-Stiftung, the Union Bank of Switzerland (Bu 704/7-1), and the Fridericus Stiftung, FL-9490, Vaduz.

Submitted: 28 December 2000
Revised: 27 March 2001
Accepted: 19 April 2001

REFERENCES

Akabas, M.H., C. Kaufmann, P. Archdeacon, and A. Karlin. 1994. Identification of acetylcholine receptor channel-lining residues in the entire M2 segment of the alpha subunit. *Neuron.* 13:919–927.

Akabas, M.H., D.A. Stauffer, M. Xu, and A. Karlin. 1992. Acetylcholine receptor channel structure probed in cysteine-substitution mutants. *Science.* 258:307–310.

Bertrand, D., and Ch. Bader. 1986. DATAC: a multipurpose biological data analysis program based on a mathematical interpreter. *Int. J. Bio-med. Comput.* 18:193-202.

Busch, A., S. Waldegger, T. Herzer, J. Biber, D. Markovich, G. Hayes, H. Murer, and F. Lang. 1994. Electrophysiological analysis of Na^+/P_i cotransport mediated by a transporter cloned from rat kidney and expressed in Xenopus oocytes. *Proc. Natl. Acad. Sci. USA.* 91: 8205-8208.

Busch, A.E., C.A. Wagner, A. Schuster, S. Waldegger, J. Biber, H. Murer, and F. Lang. 1995. Properties of electrogenic P_i transport by a human renal brush border Na^+/P_i transporter. *J. Am. Soc. Nephrol.* 6:1547–1551.

Custer, M., M. Lötscher, J. Biber, M. Murer, and B. Kaissling. 1994. Expression of Na-P_i cotransport in rat kidney: localization by RT-PCR and immunohistochemistry. *Am. J. Physiol.* 266:F767–F774.

Doyle, D.A., J.M. Cabral, R.A. Pfuetzer, A. Kuo, J.M. Gulbis, S.L. Cohen, B.T. Chait, and R. MacKinnon. 1998. The structure of the po-

tassium channel: molecular basis for K^+ conduction and selectivity. *Science.* 280:69–77.

Forster, I., N. Hernando, J. Biber, and H. Murer. 1998. The voltage dependence of a cloned mammalian renal type II Na^+/P_i cotransporter (NaPi-2). *J. Gen. Physiol.* 112:1–18.

Forster, I., D.D.F. Loo, and S. Eskandari. 1999a. Stoichiometry and Na^+ binding cooperativity of rat and flounder renal type II Na^+-P_i cotransporters. *Am. J. Physiol.* 276:F644–F649.

Forster, I.C., M. Traebert, M. Jankowski, G. Stange, J. Biber, and H. Murer. 1999b. Protein kinase C activators induce membrane retrieval of type II Na^+-phosphate cotransporters expressed in Xenopus oocytes. *J. Physiol.* 517:327–340.

Forster, I.C., J. Biber, and M. Murer. 2000. Proton sensitive interactions with the type II Na^+/P_i cotransporter. *Biophys. J.* 79:215–230.

Frillingos, S., M. Sahin-Toth, J. Wu, and H.R. Kaback. 1998. Cys-scanning mutagenesis: a novel approach to structure-function relationships in ploytopic membrane proteins. *FASEB J.* 12:1281–1299.

Grunewald, M., and I.B. Kanner. 2000. The accessibility of a novel reentrant loop of the glutamate transporter GLT-1 is restricted by its substrate. *J. Biol. Chem.* 275:9684–9689.

Hartmann, C.M., C.A. Wagner, A.E. Busch, D. Markovich, J. Biber, F. Lang, and H. Murer. 1995. Transport characteristics of a murine renal Na^+/P_i cotransporter. *Pflügers Arch.* 430:830–836.

Hayes, G., A. Busch, M. Lötscher, S. Waldegger, F. Lang, F. Verrey, J. Biber, and H. Murer. 1994. Role of N-linked glycosylation in rat renal Na/Pi cotransport. *J. Biol. Chem.* 269:24143–24149.

Holmgren, M., Y. Liu, Y. Xu, and G. Yellen. 1996. On the use of thiol-modifying agents to determine channel topology. *Neuropharmacology.* 35:797–804.

de la Horra, C., N. Hernando, G. Lambert, I. Forster, J. Biber, and H. Murer. 2000. Molecular determinants of pH sensitivity of the type IIa Na/Pi cotransporter. *J. Biol. Chem.* 275:6284–6287.

de la Horra, C., N. Hernando, G. Lambert, I. Forster, J. Biber, and H. Murer. 2001. Molecular determinants of Na^+ affinity of the type IIa Na/P_i cotransporter. *J. Physiol.* 531:383–391.

Iwaki, S., N. Tamura, T. Kimura-Someya, N. Shigeyuki, and A. Yamaguchi. 2000. Cysteine-scanning mutagenesis of transmembrane segments 4 and 5 of the Tn10-encoded metal-tetracycline/H^+ antiporter reveals a permeability barrier in the middle of a transmembrane water-filled channel. *J. Biol. Chem.* 275:22704–22712.

Javitch, J. 1998. Probing structure of neurotransmitter transporters by substituted-cysteine accessibility method. *Methods Enzymol.* 296: 332–346.

Kaback, H.R. 1997. A molecular mechanism for energy coupling in a membrane transport protein, the lactose permease of Escherichia coli. *Proc. Natl. Acad. Sci. USA.* 94:5539–5543.

Kaplan, R.S., J. Mayor, D. Brauer, R. Kotaria, D.E. Walters, and A. Dean. 2000. The yeast mitochondrial citrate transport protein. *J. Biol. Chem.* 275:12009–12016.

Karlin, A., and M. Akabas. 1998. Substituted-Cysteine Accessibility Method. *Methods Enzymol.* 293:123–145.

Kempson, S.A. 1988. Novel specific inhibitors of epithelial phosphate transport. *NIPS.* 3:154–157.

Lambert, G., I.C. Forster, J. Biber, and H. Murer. 1999a. Properties of the mutant Ser-460-Cys implicate this site in a functionally important region of the type IIa Na^+/P_i cotransporter protein. *J. Gen. Physiol.* 114:637–651.

Lambert, G., M. Traebert, N. Hernando, J. Biber, and H. Murer. 1999b. Studies on the topology of the renal type II NaPi-cotransporter. *Pflügers Arch.* 437:972–978.

Lambert, G., I.C. Forster, J. Biber, and H. Murer. 2000a. Cysteine residues and the structure of the rat renal proximal tubular type II sodium phosphate cotransporter (Rat Napi-IIa). *J. Membrane Biol.* 176:133–141.

Lambert, G., M. Traebert, J. Biber, and H. Murer. 2000b. Cleavage of disulfide bonds leads to inactivation and degradation of the type IIa, but not type IIb sodium phosphate cotransporter expressed in Xenopus laevis oocytes. *J. Membrane Biol.* 176:143–149.

Lo, B., and M. Silverman. 1998a. Replacement of Ala-166 with cysteine in the high affinity rabbit sodium/glucose transporter alters transport kinetics and allows methanethiosulfonate ethylamine to inhibit transporter function. *J. Biol. Chem.* 273:903–909.

Lo, B., and M. Silverman. 1998b. Cysteine scanning mutagenesis of the segment between putative transmembrane helices IV and V of the high affinity Na^+/glucose cotransporter SGLT1. *J. Biol. Chem.* 273:29341–29351.

Loo, D.D.F., A. Hazama, S. Supplisson, E. Turk, and E.M. Wright. 1993. Relaxation kinetics of the Na^+/glucose cotransporter. *Proc. Natl. Acad. Sci. USA.* 90:5767–5771.

Loo, D.D., B.A. Hirayama, E.M. Gallardo, J.T. Lam, E. Turk, and E.M. Wright. 1998. Conformational changes couple Na^+ and glucose transport. *Proc. Natl. Acad. Sci. USA.* 95:7789–7794.

MacKinnon, R. 1995. Pore loops: an emerging theme in ion channel structure. *Neuron.* 14:889–892.

Magagnin, S., A. Werner, D. Markovich, V. Sorribas, G. Stange, J. Biber, and H. Murer. 1993. Expression cloning of human and rat renal cortex Na/P_i cotransport. *Proc. Natl. Acad. Sci. USA.* 90:5979–5983.

Mordoch, S.S., D. Granot, M. Lebendiker, and S. Schuldiner. 1999. Scanning cysteine accessibility of EmrE, an H^+-coupled multidrug transporter from Escherichia coli, reveals a hydrophobic pathway for solutes. *J. Biol. Chem.* 274:19480–19486.

Murata, K., K. Mitsuoka, T. Hirai, T. Walz, P. Agre, J.B. Heyermann, A. Engel and Y. Fujiyoshi. 2000. Structural determinants of water permeation through aquaporin-1. *Nature.* 407:599–605.

Murer, H., N. Hernando, I. Forster, and J. Biber. 2000. Proximal tubular phosphate reabsorption: Molecular mechanisms. *Physiol. Rev.* 80:1373–1409.

Pascual, J.M., and A. Karlin. 1998. State-dependent accessibility and electrostatic potential in the channel of the acetylcholine receptor. *J. Gen. Physiol.* 111:717–739.

Sambrook, J., E.F. Fritsch, and A.M. Maniatis. 1989. Molecular Cloning- a Laboratory Manual, C. Nolan, editor. Cold Spring Harbor Laboratory, Cold Spring Harbor NY. 18.66-18.75.

Seal, R.P., and S.G. Amara. 1998. A reentrant loop domain in the glutamate carrier EAAT1 participates in substrate binding and translocation. *Neuron.* 21:1487–1498.

Silverman, M. 2000. Glucose reabsorption in the kidney: molecular mechanism of the Na^+/glucose cotransporter. *In* The Kidney, Physiology and Pathophysiology, D.W. Seldin and G. Giebisch, G. editors. Raven, New York. 2168-2178.

Turk, E., C.J. Kerner, M.P. Lostao, and E.M. Wright. 1996. Membrane topology of the human Na^+/glucose cotransporter SGLT1. *J. Biol. Chem.* 271:1925–1934.

Werner, A., J. Biber, J. Forgo, M. Palacin, and H. Murer. 1990. Expression of renal transport systems for inorganic phosphate and sulfate in *Xenopus laevis* oocytes. *J. Biol. Chem.* 265:12331–12336.

Wakabayashi, S., P. Tianxiang, X. Su, and M. Shigekawa. 2000. A novel topology model of the human Na^+/H^+ exchanger isoform 1. *J. Biol. Chem.* 275:7942–7949.

Yu, N., Y. Cao, S. Mager, and H.A. Lester. 1998. Topological localization of cysteine 74 in the GABA transporter, GAT1, and its importance in ion binding and permeation. *FEBS Letters.* 426:174–178.